LUNAR LASER RANGING: A CONTINUING LEGACY OF THE APOLLO PROGRAM

J. O. Dickey[1], P. L. Bender[2], J. E. Faller[2], X X Newhall[1], R. L. Ricklefs[3], J. G. Ries[3], P. J. Shelus[3], C. Veillet[4], A. L. Whipple[3], J. R. Wiant[3], J. G. Williams[1] and C. F. Yoder[1]

[1]Jet Propulsion Laboratory
4800 Oak Grove Drive
MS 238-332
Pasadena, CA 91109

[2]Joint Institute for Laboratory Astrophysics
University of Colorado and
National Institute of Standards and Technology
Boulder, CO 80309-0440

[3]University of Texas - Austin
McDonald Laser Ranging Operations
McDonald Observatory/Astronomy
Austin, TX 78712-1083

[4]OCA/CERGA
Avenue Copernic
Grasse F-06130
France

Invited Review Article submitted to *Science*

January 18, 1994

Outline

Abstract

On July 21, 1969, the first manned lunar mission, Apollo 11, placed the first retroreflector array on the Moon, enabling highly accurate measurements of the Earth-Moon separation via laser ranging. The past quarter century has witnessed a period of achievement and scientific impact for Lunar Laser Ranging (LLR), with the promise of continued future contributions evident. LLR, which utilizes laser ranging to the Earth's natural satellite as a laboratory for a broad range of investigations, has influenced astronomy, lunar science, gravitational physics, geodesy, and geodynamics. Unique contributions from LLR include the following: the revolutionary breakthrough in the lunar ephemeris, with a three-orders-of-magnitude improvement in accuracy; a several-orders-of-magnitude improvement in the measurement of the variations in the Moon's rotation; and the verification of the principle of equivalence for massive bodies with unprecedented accuracy. LLR analysis has provided measurements of the Earth's precession, the Moon's tidal acceleration, and lunar rotational dissipation. The scientific results, current technological developments and prospects for the future, are discussed here.

1. Introduction

It has been nearly a quarter century since the first manned lunar landing by the Apollo 11 astronauts. Included on that mission and the later Apollo 14 and 15 flights were corner-cube retroreflector arrays (Fig. 1) that permit accurate laser measurement of the Earth-Moon separation. The locations of the three Apollo arrays plus a French-built array on the Soviet roving vehicle Lunakhod 2 provide a favorable geometry for studying the rotations of the Moon and for separating these rotations from lunar orbital motion and geodynamic effects (Fig. 2, Table 1). Unlike the other Apollo scientific experiments, these retroreflector arrays require no power and are still operating normally after 25 years.

LLR has proven to be a valuable multidisciplinary tool, advancing many areas of science. Several reviews have addressed these contributions: Bender *et al.* (1) mark the transition of the LLR program from a mission experiment to one of scientific exploration; Williams (2) outlines the early scientific accomplishments; Mulholland (3) reviews the progress made during the first decade of LLR; and Alley (4) discusses LLR results as a test of gravitational theories. Dickey *et al.* (5) and Whipple (6) highlight the accomplishments and future challenges for LLR; Williams *et al.* (7) document geophysical results and reference frame contributions from LLR.

In this paper we review LLR technological developments and scientific results. A description of the data characteristics and the enabling technological developments is presented in Section 2. Analysis procedures and scientific results are reviewed in Section 3 with respect to four broad areas: (1) ephemeris development and related activity, 2) gravitational physics, (3) geodynamics, and (4) lunar science. Concluding remarks and prospects for the future are given in the final section.

2. Data Characteristics and Technology Development

Lunar laser ranging consists of transmitting short pulses of light to the Moon, where they are reflected back to their source. By noting the round-trip travel time, the transmitter-reflector separation is measured. Changes of the round-trip travel time (or the equivalent distance) with time contain, and yield on analysis, a wealth of information about the Earth-Moon system. The range data contain a rich frequency spectrum due to many effects such as Sun's strong influence on the lunar orbit.

Ranging to the Moon is technically challenging. An outgoing pulse of laser light transmitted from a collimating telescope with a beam divergence of 3–4 seconds of arc, consistent with atmospheric seeing, spreads to an area approximately 7 km in diameter on the lunar surface. Light which is backscattered from the laser-illuminated part of the lunar surface produces a weak, though marginally detectable, signal that has a time width

characteristic of local lunar topography. Consequently, range measurements to a given target area can vary by the order of a kilometer, which limits its applications.

The retroreflector arrays, placed on the lunar surface by the U. S. Apollo program in July of 1969 (Apollo 11) and in January and July of 1971 (Apollo 14 and 15) and the Soviet Lunakhod program using French-built retroreflectors (1971 and 1973), provide optical points on the Moon toward which one can fire a laser pulse and receive back a localized and recognizable signal. The result is that centimeter level ranging accuracies were immediately possible and meaningful, if one had sufficiently short laser pulse lengths with high power. Today, few-centimeter range accuracy for "normal points" corresponding to the results over periods of 10–45 min (8) is being obtained routinely.

The design of the Apollo and Lunakhod retroreflector arrays is straightforward. Each individual corner cube reflects incident light back to its point of origin. The Apollo arrays consist of 100 (Apollo 11 and 14) or 300 (Apollo 15) 3.8 cm diameter corner cubes mounted in an aluminum panel. The Soviet-French Lunakhod arrays consist of a smaller number, (i.e., 14) of larger corner cubes, 11 cm on an edge. Though subject to thermal distortion during the lunar day because of their greater size, they give approximately the same lunar-night return signal strength as the Apollo arrays.

The relatively small size of the arrays means that only 10^{-9} of the impinging light can be collected and therefore reflected back toward the Earth. The angular spread of the returning pulse is set by diffraction, polarization properties, and irregularities of the arrays' individual corner cubes which, in the case of the 3.8 cm diameter Apollo corner cube, is approximately 10 seconds of arc. Thus, the diameter of the spot produced on the Earth is approximately 20 km. The use of a 1-m diameter receiving telescope would mean that only 2×10^{-9} of the returning photons would enter the aperture. A variety of practical matters, such as quantum efficiency, mirror reflectance, optical performance under thermal stress, and velocity aberration (which slightly shifts the center of the returning beam from the location of the transmitting and receiving telescope), make the transmitting, lunar

retroreflecting and receiving efficiencies considerably less than unity. The signal loss of approximately 10^{-21} puts a premium on the detailed design of ground stations to minimize their losses. Since three joules of light, the most energy that one can currently transmit each second, contains 1×10^{19} photons, single-photon detection is a necessity.

At present, there are only a few lunar laser ranging stations operating, and only one of these is fully dedicated to lunar ranging. The other stations are shared lunar and artificial-satellite ranging facilities. At the time of the Apollo 11 landing, laser ranging was initiated at McDonald Observatory in Texas, where lunar ranging (shared with artificial-satellite ranging) continues. Preliminary ranging also took place at the Lick Observatory in California where the first returns from the Moon were detected (9).

During the first fifteen years after the emplacement of the initial retroreflector package on the lunar surface, the McDonald Observatory, near Fort Davis, Texas, was the only facility that routinely ranged to the Moon. In the late 1960s, the new 2.7-m telescope had just become operational at McDonald, and a commitment to use this instrument in a long-term program of lunar laser ranging was made. Time-sharing with the Observatory's regular astronomical program, McDonald laser operations maintained routine activities for more than 15 years. There were nominally three 45-minute observing sessions per day, when the Moon was 3 hours east of, on, and 3 hours west of the meridian, some 21 days per lunation (10). The data can naturally be divided into three time spans, based on their accuracies (see Fig. 3). The early 1970s saw LLR data accuracies at the 25 cm level. Based mainly upon improvements in the 2.7-m LLR timing system, these were improved to the 15 cm level by the mid-1970s. When the transition was made in the mid-1980s to the MLRS LLR system, accuracies were further improved to the 2-3 cm level. Despite the order-of-magnitude improvement in accuracy during the past two decades, the early data are still important in the separation of effects with long characteristic time scales, notably precession and nutation, relativistic geodetic precession, tidal acceleration, lunar J_2, and the relative orientation of the planes of the Earth's equator, the lunar orbit and the ecliptic.

The 2.7-m McDonald laser ranging system was decommissioned in 1985 and was superseded by a dedicated 0.76-m ranging system, the McDonald Laser Ranging System (MLRS) capable of ranging to artificial satellites as well as to the Moon (11—see Fig. 4). The present incarnation of the MLRS is constructed around a frequency-doubled, 120 millijoules/pulse, 200 picosecond pulse-length, neodymium-YAG laser firing 10 times/second. It has an internal calibration system, and the precision of its epoch timing system is approximately 25 picoseconds. This station now produces LLR data approaching 1 cm normal-point precision. However, the accuracy is still limited to 2–3 cm. In spite of its reduced aperture, which results in fewer data than the 2.7-m telescope could have produced, the shorter laser pulse length has led to a fourfold improvement in the accuracy of the MLRS ranges, providing stronger data than those from the 2.7 meter system despite the reduced volume. A number of strategies are being pursued to produce significantly higher volumes of LLR data and further increases in accuracy, including increased station computing, offset guiding and tracking, and improved timing systems.

During the past 8 years, successful ranging has been carried out by a French (CERGA) station at Grasse, located at 1220 m elevation 20 km north of Cannes, using a 1.5-m dedicated lunar laser ranging telescope, and until recently by a second U.S. artificial-satellite and lunar ranging station on Maui, Hawaii. Though strong lunar returns were often received by this latter station—a station which continues to perform artificial satellite ranging—it has been unable to continue lunar ranging during the past few years due to cutbacks in available support. The Grasse site has a dedicated lunar station equipped with a 1.5-m telescope with both absolute and offset pointing capabilities; a separate artificial satellite ranging facility is located nearby (12). The station's 10 Hz repetition rate Nd YAG laser produces 700 mJoules per pulse at 1.064 μm. The yield on frequency doubling is half of this energy at 0.532 μm—the rest remains as infrared (IR). The pulse length (at half height) is 350 picoseconds, giving a transmitted pulse length of approximately 0.1m. Technological innovations and upgrades that have occurred at the Grasse station include

experimental simultaneous ranging in the green and IR and the use of high speed and high quantum efficiency photodiodes (instead of photomultipliers) for detectors. During the past 5 years, this dedicated station has produced the bulk of lunar ranging data, with 2–3 cm accuracy. Lunar laser ranging has also been occasionally carried out from (primarily) artificial satellite stations in Australia and Germany, and has been proposed at several other stations around the world. Data from a global network of stations (Table 1) are clearly needed for a robust analysis program since separation of parameters is enhanced by a geographically distributed network of observing sites.

3. Analysis and the Impact of LLR on Various Disciplines

The data set that will be considered here consists of over 8,200 normal-point ranges (8) spanning the period August 1969–December 1993. The observatories and the lunar reflectors included in the analysis are listed in Table 1, with time history of returns shown in Fig. 5. The data are analyzed with a model which calculates the light travel time between the observatory and the reflector, accounting for the orientation of the Earth and Moon, the distance between the centers of the two bodies, solid tides on both bodies, plate motion, atmospheric delay, and relativity (13). The parameters (Table 2) which have been fit include the geocentric locations of the observatories, corrections to the variation of latitude (i.e., polar motion), the orbit of the Moon about the Earth, the Earth's obliquity, precession, and nutation, plus lunar parameters including the selenocentric reflector coordinates, fractional moment-of-inertia differences, gravitational third-degree harmonics, a lunar Love number, and rotational dissipation.

Orbits and Ephemeris Development

The computation of the round trip light travel time between the ranging observatory and the lunar reflector depends on the geocentric location of the observatory $\mathbf{R_E}$, the selenocentric position of the reflector $\mathbf{R_M}$, and the distance between the centers of the Earth

and Moon **r**. For data analysis, the light time calculation is done with higher accuracy, but for purposes of discussion the approximate range (see Fig. 6) is:

$$\rho \simeq |\mathbf{r}| - \mathbf{R_M} \cdot \hat{\mathbf{r}} + \mathbf{R_E} \cdot \hat{\mathbf{r}} \qquad (1)$$

The mean Earth-Moon distance is 384,400 km; the radii of the Earth and Moon are 6371 km and 1738 km, respectively.

The Moon's orbit is strongly distorted from a simple elliptical path by the solar attraction—the instantaneous eccentricity varies by a factor of two (0.03 to 0.07). The perturbed orbit contributes a rich spectrum of range signatures which give sensitivity to a wide variety of parameters. The complications of the orbit are handled by simultaneous numerical integration of the orbits of the Moon and nine planets (the lunar and planetary ephemeris), and lunar rotation (lunar librations) (14). While our numerical integrations use Cartesian coordinates rather than orbital elements as explicit parameters, analytical theories fit to the integrations provide information on the behavior of the orbital elements (15). The accuracy of the resulting ephemeris is set by the accuracy of the model for accelerations and the accuracy of the fit of the range data. The lunar ephemeris relies entirely on LLR data. The existing acceleration model accounts for relativistic forces between the Sun, Earth, Moon and planets; gravitational harmonics of the Earth and Moon; the orientation of the Earth's equator; the rotation of the triaxial Moon (physical librations); tides, including tidal dissipation of energy on both Earth and Moon; and gravitational forces from the larger asteroids. The associated parameters such as masses, gravitational harmonic coefficients, and tidal strengths must be known a priori or must be included among the parameters fit in the least-squares solution to the time delay measurements.

From the solution, the lunar orbit about the Earth is determined with great accuracy. Ranging data have provided a dramatic improvement in the accuracy of the lunar orbit: the orientation is determined at least two orders of magnitude more accurately, and the accuracy of the radial component is better by four orders of magnitude, than that obtained from classical optical data. The radial distance variations are determined better than the 2–3 cm

range accuracy. The angular-rate uncertainty is no more than 0.3 milliseconds of arc/yr (7). The orbital components having the greatest uncertainties are the mean distance, presently 0.8 m due to correlation with the reflector coordinates in the mean-Earth direction, and the orientation of the orbit plane with respect to the Earth's equator, 1.5 milliseconds of arc or 3 m at the lunar distance. These accuracies are degraded when extrapolated outside the span of observations. A continual supply of high-quality measurements and the accompanying analysis are required to maintain and enhance accuracies. The ephemerides and physical librations are essential for mission planning and spacecraft navigation.

The strong influence of the Sun on the lunar orbit permits the range data to be used to determine the mass ratio Sun/(Earth+Moon) and the relative orientation of the Earth-Moon system orbit about the Sun. The size of the Earth-Moon orbit is set by the sum of the Earth's GM and the Moon's GM, with the Moon's orbit being deformed from a simple Keplerian ellipse by the influence of the Sun. The two largest solar perturbations in distance **r** are 3,699 km (monthly) and 2,956 km (semimonthly), and few centimeter determination of these variations corresponds to 10^{-8} relative accuracy in the mass ratio (16). From fits, the mass ratio is found to be (7)

$$\text{Mass}_{\text{Sun}} / \text{Mass}_{(\text{Earth + Moon})} = 328900.560 \pm 0.002$$

The solar perturbations allow the relative geocentric positions of the Moon and Sun to be determined to within one millisecond of arc. The planetary positions are known with respect to the Earth's orbit around the Sun, so the geocentric position of the Moon and the heliocentric positions of the planets can be made internally consistent in their relative orientation (17). Because the ranging stations are on the spinning Earth, the orientation of the equatorial plane is also determined relative to both the lunar orbit plane and the ecliptic plane of the heliocentric Earth-Moon orbit. Thus, LLR is sensitive to the mutual orientation of the planes of the Earth's equator, the lunar orbit, and the ecliptic; hence, it locates the intersection of the ecliptic and equator planes (the dynamical equinox) and determines the

angle between them (the obliquity of the ecliptic). The process of orienting the planetary ephemerides into the fundamental astronomical reference frame is made possible at the millisecond of arc level with LLR data (18).

Gravitational Physics and Relativity

Lunar laser ranges, along with microwave ranges to planetary orbiting spacecraft and landers, have contributed strongly to solar system tests of gravitational theories. The Moon and planets provide excellent tests, because the ratio of non-gravitational to gravitational forces is very small. For example, the ratio of the solar radiation pressure force on the Moon to the gravitational attraction by the Earth is only 4×10^{-13}.

Shortly before the first Apollo landing, Nordtvedt (19) pointed out that a new test of general relativity could be carried out using lunar range data. The equivalence principle, a fundamental tenet of general relativity, states that the ratio of gravitational mass to inertial mass is the same for all bodies, independent of their composition (20). This principle had been tested in the laboratory but had not been tested for bodies large enough to have a significant fraction of their mass coming from gravitational self-energy. The Strong Equivalence Principle in gravitational theory requires that all bodies fall with the same acceleration in an external gravitational field, with the gravitational self-energy contributing equally to the gravitational and inertial masses. Different metric theories of gravitation treat the effect of gravity on gravitational energy differently; some predict violations of the Strong Equivalence Principle by massive bodies (21).

Since 1976, lunar laser ranging data have been used to test the Strong Equivalence Principle (22). If the Earth and the Moon were separately orbiting the Sun with the same period, a violation of the Principle would lead to their having different mean distances from the Sun. This is because roughly 4.64×10^{-10} of the mass of the Earth is due to its gravitational self-energy, i.e., the gravitational interaction energy of its different parts, while the corresponding fraction for the Moon is much less (1.9×10^{-11}). In the actual

situation, where the Moon orbits the Earth, a violation of the Equivalence Principle would cause the orbit of the Moon about the Earth-Moon center of mass to be polarized in the direction of the Sun, with the maximum size of the polarization being about 9 m (see Fig. 7). This signature would have the synodic period of 29.53 days and is referred to as the Nordtvedt term:

$$\delta r = C_0 \eta \cos D,$$

where D is the angular elongation of the Moon from the Sun and $C_0 \sim 9$m. The quantity η is defined by the ratio of gravitational mass M_G to the inertial mass M_I:

$$M_G / M_I = 1 + \eta U_G / Mc^2,$$

where U_G is the self-energy (23, 24) and c is the speed of light. Analysis with the early LLR data up to the mid-1970s confirmed General Relativity with $\eta = 0.00 \pm 0.03$ (22). The current determination of the polarization of the lunar orbit from lunar laser ranging data gives a value of $C_0\eta = -0.5 \pm 1.3$ cm (or $\eta = -0.0006 \pm 0.0014$), which is currently the best test of the Strong Equivalence Principle. Here, the errors are realistic rather than formal (25). This uncertainty is about a factor 5 less than reported previously (26, 27). With feasible improvements in the accuracy for lunar ranging (see final section), and with continued data, further improvement in the test appears likely.

The above results can be interpreted as a test of the parameters β and γ from the Parametrized Post Newtonian theory of gravitation, which in General Relativity has the value of $\beta = \gamma = 1$. The Nordtvedt coefficient, η, can be expressed as:

$$\eta = 4\beta - 3 - \gamma .$$

The parameter β measures the superposition of gravitational effects, and usually is thought of as determined from the precession of perihelion for Mercury, while γ measures how much space-curvature is produced by unit rest mass (20). Combining the above value for η with the result $\gamma = 1.000 \pm 0.002$ from analysis of the Viking lander tracking data (28) gives

$$\beta = 0.9999 \pm 0.0006.$$

The uncertainty is about a factor of 5 smaller than if β is derived from the precession of Mercury's perihelion (27).

A second important test of gravitational theory comes from the measurement of relativistic precession of the lunar orbit (termed geodetic precession), first predicted by de Sitter in 1916. According to General Relativity, this effect should cause a precession of the entire lunar orbit with respect to the inertial frame of the solar system by 19 milliseconds of arc/yr. The lunar range data are sensitive to this effect mainly through the excess precession of perigee beyond that expected due to the Newtonian effects of the Sun, Earth, and other planets (29). The first observations of geodetic precession did not occur until the late 1980's; those results were in agreement with the predictions of General Relativity to within their 2% accuracy (30, 26). New solutions presented here (Table 3) give a difference from the expected value of $-0.3 \pm 0.9\%$. The error is partly due to an uncertainty in J_2, the primary lunar oblateness term (31).

Lunar range data also provide a test of a possible change in the gravitational constant (G) with time because of the lunar orbit sensitivity to solar longitude (16). Adding cosmological interest is the suggestion that quite large changes in G may have occurred during an inflationary phase in the early history of the universe (see e. g. 32). Estimates of limits on $dG/dt \,/\, G$ from combining various types of solar system data including lunar data and Viking lander tracking data currently range from 1×10^{-11}/yr to 0.4×10^{-11}/yr (33, 34). The published limit from binary pulsar data is 1.3×10^{-11}/yr (35). Our current uncertainty from analyzing lunar range data only is similar to that reported by Chandler et al. (33).

Geodynamics

Of importance to the geodynamics community has been the series of LLR measurements that permit long-term studies of variations in the Earth's rotation, as well as the determination of constants of precession and nutation, station coordinates and motions,

the Earth's gravitational coefficient, and tides accelerating the Moon (6,7). For studying the processes which underlie variations in the Earth's rotation, the more than two-decade-long span of LLR data exceeds that available from other space geodetic techniques. LLR has provided information about the exchange of angular momentum between the solid Earth and the atmosphere (36) and was instrumental in the discovery of the near 50-day oscillation in the length of day and its correlation with a similar oscillation in the atmosphere (37), which has stimulated research in the atmospheric community (38). Tidally driven periodic terms in Earth rotation have been studied and have been used to determine the response of the Earth (dependent on the Earth's structure and tides) at the fortnightly and monthly periods (39). The development of regular very-long-baseline interferometry (VLBI) measurement programs during the 1980s and refinement of satellite laser ranging programs have strongly complemented LLR results, providing more frequent and regular measurements in recent years (36).

LLR provides an accurate value of the mass ratio Sun/(Earth + Moon) (see previous section on orbits). Utilizing this mass ratio together with the solar GM and the lunar GM from lunar-orbiting spacecraft (40), the Earth's GM (7) in an Earth-centered reference frame is determined with accuracy of 1 part in 10^8 (see Table 4). Within the errors, this value is compatible with the value derived from ranges to artificial Earth satellites (41).

Tidal dissipation causes a misalignment of the tidal bulge of the Earth relative to the Earth-Moon direction. The bulge exerts a secular torque, causing the lunar orbit to expand as its angular momentum increases and the Earth's rotation rate to decrease. Most of the effect comes from the ocean tides, but a small unknown contribution comes from the mantle. The importance of this tidal acceleration of the Moon is that it is the dominant cause of the long-term slowing of the Earth's rotation rate (other contributors are the tidal interaction with the Sun and the change in the Earth's oblateness). The resulting changed length-of-day has been seen in the geological record in a few special circumstances (42).

Because the lunar orbit is neither circular nor coplanar with the Earth's equator, the tides can be separated into distinct frequency components within bands near 0, 1, and 2 cycles/day. The tidally induced secular acceleration $\dot{n}$ of the lunar mean longitude is due mainly to the dominant semi-diurnal M_2 constituent, with smaller contributions from the diurnal O_1 and semi-diurnal N_2 components. The span and accuracy of the data are now sufficient to resolve the diurnal and semi-diurnal contributions from the amplitude of the 18.6 year along track tidal perturbations (43). The diurnal contribution is -4.04 ± 0.4 arcsec/cy^2; the semi-diurnal tides contribute -22.24 ± 0.6 arcsec/cy^2 for a total of -26.28 ± 0.5 arcsec/cy^2 (44). The small dissipation in the long-period tides is not modeled and is effectively included in the semi-diurnal component. This LLR-derived secular acceleration is compatible with those inferred from artificial satellite measurements of ocean tides (45) for both the diurnal and semidiurnal components. Dissipation in the Moon itself is well established, but the contribution to the secular acceleration depends on which of two possible mechanisms of dissipation dominates: solid friction modeled by a constant time delay or turbulent fluid friction at the lunar core-mantle boundary (see following section). The time-delay lunar model utilized (46, 47) causes +0.4 arcsec/cy^2, yielding a total secular acceleration of -25.88 ± 0.5 arcsec/cy^2. If the dissipation is due to fluid friction at a core-mantle interface (44), the lunar contribution could be considerably smaller. The total tidal secular acceleration corresponds to an increase in the semimajor axis of 3.82 ± 0.07 cm/yr.

Due to torques from the Sun and Moon, the Earth's spin axis precesses about the ecliptic periodically and nutates in space. These motions, designated luni-solar precession and nutation, respectively, depend on the flattening of the Earth [more specifically, the moment of inertia function (C-A)/C], the flattening of the core-mantle interface, and ocean tides. Both LLR and VLBI analyses (7, 48, 49) have indicated that significant corrections are required to the standard precession and nutation model, as a consequence of geophysical effects. The nearly quarter-century span of the LLR observations is an advantage when trying to detect and separate the precession and 18.6 yr nutation

corrections; LLR analysis indicates that the correction to the standard precession constant is -3.3 ± 0.4 milliseconds of arc/yr (7), giving the lunar-solar precession constant as 50.3845 seconds of arc/yr. Further, the amplitude of the 18.6 yr nutation in-phase term of the pole requires a correction of about 3 milliseconds of arc, the magnitude of the term being increased, with a smaller out-of-phase term. Also detected was a 2 milliseconds of arc annual correction (7, 48, 49), which has been interpreted as being due to a 5% deviation in the flattening of the core-mantle boundary from that expected from hydrostatic equilibrium (50). An analogous discrepancy between theory and observation has been observed in tidal gravity data (51), with results which are consistent with this increased flattening of 5%. Joint solutions for precession and nutation have been made using LLR and VLBI data together, which combine the strength of the LLR data for the long time scale with the high resolution of the VLBI data for shorter periods (52).

Lunar Science

The analysis of the LLR data provides a wealth of information concerning the dynamics and structure of the Moon. The selenocentric reflector coordinates, the moment of inertia combinations, $\beta = (C-A)/B$ and $\gamma = (B-A)/C$ (where $A < B < C$), and the third-degree gravitational harmonics are determined with high accuracy. The coordinates for the lunar reflectors and the ALSEP radio transmitters serve as the fundamental control points for lunar cartography (53). The distances between the retroreflectors and the Earth change in part due to lunar rotation (physical librations) and tides. Values of the gravitational harmonics, the moments of inertia and their differences, the lunar Love number k_2 (which measures the tidal change in the moments of inertia and gravity—see Table 5) and variations in the lunar physical librations are related to the Moon's composition, mass distribution, and internal dynamics.

Presently, the most accurate estimate of the lunar moment of inertia is obtained from the separate determinations of moment of inertia differences, β and γ, from the LLR

solution (see Table 5) and the lunar gravity field coefficients, J_2 [=(C–(B+A)/2)/MR^2] and C_{22}[=(B–A)/4MR^2] obtained from analysis of lunar satellite doppler data (54). The resulting polar moment from these two different data analyses is C=(0.3933 ± 0.0011)MR^2. The lunar mass distribution also perturbs the lunar orbit, producing secular precessions in the lunar node and perigee directions (55). The lunar mass distribution contributions are –0.17 arcsecond/year to the node rate and –0.02 arcsecond/year to the perigee rate; the former changes the monthly range signature in $\mathbf{R_E} \cdot \hat{\mathbf{r}}$ by 0.5 m/year.

Figure 8 shows an interpretation of the polar moment in terms of a 60km thick lunar crust with density 2.75 g/cc, a constant density (ρ) lunar upper mantle, a lower mantle with contrast in $\Delta\rho$ relative to the upper mantle and a variable radius iron core with density = 7 g/cc. We find that the maximum core size is in the range of 220–350 km. Magnetometer estimates of core size are ambiguous. Russell *et al.* (56) find 435 ± 15 km, while Wiskerchen and Sonnet (57) claim only an upper bound of 400 km. The seismic constraint is less confining (58) with $R_c < 500$ km.

Two other major types of information concerning the lunar interior can be obtained from lunar libration data. One is the apparent tidal distortion of the Moon. The other is the mean direction of the spin axis. However, there are complications involved in interpreting the results.

Consider the influences on lunar orientation arising from: 1) inelastic deformation of the mantle shape with amplitude proportional to the tidal Love number k_2 and phase determined by the solid friction Q; 2) turbulent dissipation at the core mantle boundary (CMB) for a fluid core, and 3) CMB ellipticity e_c = (a–c)/a. The primary lunar contribution to orientation variations is dependent on the mean lunar argument of latitude F (orbital mean longitude minus the ascending node on the ecliptic). The primary latitude variations along the Earth-Moon direction (p_1) due to these effects (46, 47, 59) are

$$p_1 = (74\ k_2 + 4.9\ \frac{x}{1-x}\ (\frac{R_c}{350km})^5)\ \sin F + (230\ k_2/Q + 4.9\ \frac{y}{1+y^2}\ (\frac{R_c}{350km})^5)\ \cos F,$$

where we have adopted a core density = 7 g/cc and the units are seconds of arc. Here x = $e_c/0.0040$ is the CMB ellipticity multiplied by the ratio of the 18.6 year nodal precession period to the lunar orbit period [60], and y is the core frictional parameter to be discussed later.

The apparent Love number k_2 (Table 5) presently obtained from LLR analysis, 0.0302 ± 0.0012, comes from the coefficient of the sin F term in p, ignoring the possible CMB ellipticity. It is much larger than expected, based on naive extensions of lunar seismic velocity profiles derived from the Apollo mission. Goins *et al.* (61) and Nakamura (58) deduced similar seismic velocity profiles in the upper mantle, strikingly different profiles in the middle mantle, and provided essentially no constraints below ~ 1000 km depth. This is partially due to the front-side cluster of seismic stations, the sparsity of detectable far-side impacts, and the ~ 1000 km maximum depth of deep focus moonquakes. If we simply extend the observed S and P wave velocities down to a nominal 350 km radius core, we obtain the following model values for k_2,

$$k_2 \text{ (Goins } et\ al.\text{)} = 0.024,$$

$$k_2 \text{ (Nakamura)} = 0.022.$$

Figure 9 shows k_2 deduced from different S-wave velocities (V_s) and lunar core sizes of radius 300 and 400 km used in the Goins *et al.* (61) and Nakamara (58) models below 1000 km depth (note the lunar radius is 1738 km). The 400 km core radius corresponds to the largest possible lunar core consistent with moment of inertia and magnetic constraints. The core size, within the limits considered, has only a small effect on k_2 (62). On the other hand, if a low velocity zone below 1000 km in depth is added to the Goins *et al.* model then the observed k_2 would be consistent with $V_s \simeq 3.0$km/s. The ~ 40% decrease in V_s from middle mantle values can be explained only as arising from considerable partial melt, a much higher fraction than observed in a similar zone within the Earth. Clearly, the situation is even more implausible if the starting point is Nakamura's S-wave profile. Also, a large partial melt zone may face serious theoretical objections.

An alternative explanation for the apparent large k_2 is the presence of a small core boundary ellipticity $e_c = (a-c)/a$ which can partially mimic the k_2 libration signature, as can be seen from the equation for p_1. The observed $k_2 = 0.0302$ (with $x = 0$) can be reduced to a value of 0.024 by adopting a core radius = 350 km and a core ellipticity $a-c = 0.0004a$ = 140m. Separation of the k_2 value and core ellipticity effects depends on detection of other periodic terms which are smaller. Therefore, a solution to this problem requires improvement in range accuracy.

If the Moon were a perfectly rigid body, the mean direction of its spin axis would precess with the orbit. The lunar laser data show that the true spin axis of the Moon is displaced from this expected direction by 0.26 arcsec (Fig. 10). The two dissipative terms proportional to cos F in the expression for P_1 are due to solid and fluid dissipation. We can account for the observed 0.26 arcsec offset deduced from the lunar range by adopting either of the following: $k_2/Q = 0.001136 \pm 0.000016$ (or $Q \approx 26.5 \pm 1.0$—see Table 5) or a value for the core frictional parameter of $y = 0.053(350\text{km}/R_c)^5$ [see 63 for details]. A value of Q as low as 26.5 is surprising in view of the high seismic Q for most of the Moon, even if some partial melt is present below 1000 for depth. Thus, the presence of a fluid core with a turbulent boundary layer appears to be the plausible interpretation.

The direct separation of the competing dissipative terms is difficult. The largest differential signature arises in the lunar orbit acceleration and separation here requires an independent estimate of $\dot{n}$ due to earth tidal friction. The contribution of solid friction in the Moon to the secular $\dot{n}$ is 0.4 arcsec/century (64) while that due to core surface, fluid friction is about a factor of 3 smaller. In principle, the difference in $\dot{n}$ could be detected by comparing the total $\dot{n}$ measured by LLR with $\dot{n}$ predicted from artificial satellite measurements of ocean tides (41). Unfortunately, the present determinations are not yet precise enough to discriminate between these two alternatives.

It also is worthwhile to mention the observation of an apparent free libration of the Moon. Separate from librations driven by the time-varying torques of the Earth and Sun

(the forced physical librations), three modes of free libration exist. One of these rotational modes is analogous to the Earth's Chandler wobble (but with a 74-year period), another is an oscillation of the pole direction in space (in addition to the uniform precession), and the last is a 2.9-year oscillation in rotation speed (longitude). Without suitable recent exciting torques, and because of the substantial dissipation (see below), the amplitudes of these free librations should have damped to zero. However, the LLR data show an apparent rotational free libration in longitude for the Moon with 2.9-year period and 1 arcsec amplitude (65).

The reason why considerable uncertainty remains about this motion is that it is difficult to be certain that some very small forcing term in the lunar orbit near the resonance frequency for the free libration is not being amplified strongly to mimic the free motion. The numerically integrated rotational motions of the Moon have been compared with semi-analytic calculations of the forced angular motions to separate out the free motion; however, the semi-analytic results may not be accurate enough to rule out the observed motion actually being a forced motion.

Studies have been carried out to investigate whether the apparent free libration is likely to have been excited by impacts on the Moon (66). Such excitation would have required an impact in very recent times by an object large enough to leave a 10 km diameter crater, statistically a highly unlikely event. Seismic events on the Moon also cannot explain the observed amplitude. Passes through weak resonances have occurred in the geologically recent past and can stimulate free librations in longitude (65). A very plausible explanation appears to be core boundary effects, similar to those which are believed to account for the decade scale fluctuations in the Earth's rotation (46).

Clearly, LLR has revealed important information about lunar structure and dynamics. A continuing program will result in clear discrimination of the appropriate model interpretation, given ranging of even higher quality.

Concluding Remarks

The past quarter century has been a productive period for LLR, including several landmark scientific results such as the verification of the Strong Equivalence Principle with unprecedented accuracy, orders-of-magnitude improvements in the determination of the lunar rotation (physical librations), the indication of a probable liquid lunar core, and the accurate determination of the lunar tidal acceleration and the Earth's precession. LLR is the only working experiment which still carries forward the Apollo legacy and, because of its passive nature, can continue as long as proper ground-based ranging stations are maintained.

Over the lifetime of the LLR experiment, the range accuracy has improved by an order of magnitude from 25 cm uncertainty in the early 70s to today's 2–3 cm ranges. The precision on some days reaches 1 cm, but the calibration accuracy for the timing systems is not yet this good. The accuracy limitation due to the atmosphere appears likely to be only about 2 mm at 45° elevation angle (67).

In the immediate future, we have underway the provision of dramatically increased station computing power, offset guiding capability, and hands-off auto guiding. The benefits from the above items will not only be an increased number of normal points spread over significantly more of the lunar phase, but also a significantly increased number of individual observations within a given normal point. The more extended and denser lunar phase coverage means greater sensitivity to many of the lunar solution parameters. The increased number of observations per normal point will provide better operational precision, and hopefully aid in improving the accuracy.

Farther down the road, we see the availability of more precise and more efficient photon detectors, such as micro-channel plates, significantly improved timing systems, and shorter-pulse, more powerful lasers. These will provide for higher accuracy, additional sensitivity to lunar parameter signatures and a further increase in the lunar data density. On the more distant horizon, lunar missions have been proposed that could place microwave or

optical transponders (68) at widely separated lunar sites. This would permit differential measurements with up to two orders of magnitude improvement in accuracy.

The expected increased data density and improved accuracy in the future will permit higher understanding of the Earth, the Moon and the Earth-Moon system, answering old questions and revealing new phenomena to be explored. Advances in ephemeris development will continue, and higher improved tests of gravitational physics and relativity are expected.

References

1. P. L. Bender *et al.*, *Science,* **182**, 229 (1973).

2. J. G. Williams, in *Scientific Applications of Lunar Laser Ranging, J.* D. Mulholland, Ed. (D. Reidel, 1977), pp. 37-50.

3. J. D. Mulholland, *Rev. of Geophys. and Sp. Phys.* **18**, 3, 549 (1980).

4. C. O. Alley, in *Quantum Optics, Experimental Gravity, and Measurement Theory*, P. Meystre and M. O. Scully, Eds. (Plenum, 1983), pp. 429-495.

5. J. O. Dickey, J. G. Williams, X X Newhall, *Proceedings of the Fifth International Workshop of Laser Ranging Instrumentation*, J. Gaignebet, Ed. (Royal Greenwich Observatory, 1986), vol. 1, pp. 19-28.

6. A. L. Whipple, *Advances in Space Research* **13**, 11, 213-219 (1993).

7. J. G. Williams, X X Newhall, J. O. Dickey, *Contributions of Space Geodesy to Geodynamics: Earth Dynamics, Geodynamics Series, 24,* D. E. Smith and D. L. Turcotte, Eds., American Geophysical Union, (Washington D. C.), pp. 83-88 (1993).

8. The LLR observing process is normally broken up into individual runs for particular lunar surface retroreflectors. Each of these runs is composed of 5-100 reflections distributed over 10-45 minutes of time. The number of individual observation events grows very rapidly and, from the earliest days of the LLR experiment, data

compression into normal points has been the rule. In essence, each normal point represents the information content of an entire observation run. The complete LLR normal point construction process is described in Abbot *et al., Astron. J.*, **78**, 784-793 (1973).

9. J. Faller *et al., Science* **166**, 99 (1969).

10. Silverberg, E. C., *Appl. Opt.* **13**, 565-574, 1974; R. I. Abbot, P. J. Shelus, J. D. Mulholland and E. C. Silverberg, *Astron. Jour.* **78**, 784 (1973); P. J. Shelus, J. D. Mulholland and E. C. Silverberg, *Astron. Jour.* **80**, 154 (1975); J. D. Mulholland, P. J. Shelus and E. C. Silverberg, *Astron. Jour.* **80**, 1087 (1975).

11. P. J. Shelus, *IEEE Trans. on Geosci. and Rem. Sens.* **GE-234**, 385 (1985); P. J. Shelus, R. L. Ricklefs and A. L. Whipple, *Contributions of Space Geodesy to Geodynamics: Technology, Geodynamics Series, 25*, D. E. Smith and D. L. Turcotte, Eds., American Geophysical Union, Washington, D.C., pp. 183-187 (1993).

12. C. Veillet *et al.*, Proceedings of the Seventh International Workshop on Laser Ranging Instrumentation, C. Veillet, Ed. (Observatoire de la Côte d'Azur, Grasse, France), 149-156 (1989).

13. X X Newhall, J. G. Williams, J. O. Dickey, *Proc. International Association of Geodesy (IAG) Symposia*, 78, Bureau Central de l'A.I.G., Paris, pp. 78-82, (1987).

14. X X Newhall, E. M. Standish, J. G. Williams, *Astron. Astrophys.* **125**, 150 (1983).

15. M. Chapront-Touze and J. Chapront, *Astron. Astrophys.* **124**, 50 (1983); M. Chapront-Touze and J. Chapront, *Astron. Astrophys.* **190**, 342 (1988); M. Chapront-Touze and J. Chapront, *Lunar Tables and Programs from 4000 B. C. to A. D. 8000,* Willmann-Bell, Richmond (1991).

16. The largest four terms in the range ρ depend on $\mu = (Mass_{Earth} + Mass_{Moon})/Mass_{Sun}$ are given by:
(-3699 cos (2D – ℓ) – 2956 cos 2D + 246 cos (2D-2ℓ) – 205 cos (2D – ℓ'))km,
which provides a direct estimate of the Mass ratio μ. Determination of the phase of the terms gives D, the mean elongation of the Moon from the Sun. The variable ℓ is the mean anomaly of the Moon, while ℓ' is the mean anomaly of the Earth-Moon orbit about the Sun. In this paper, analytical equations like the above are used for disucssion, the actual analysis uses numerical partial derivatives.

17. J. G. Williams and E. M. Standish, in *Reference Frames in Astronomy and Geophysics*, J. Kovalevsky, I. I. Mueller, B. Kolaczek, Eds. (Kluwer Academic Publishers, Dordrecht, 1989), pp. 67-90.

18. Consider the component of range
$\mathbf{R_E} \cdot \hat{\mathbf{r}} \approx R_Z \sin\delta + R_S \cos\delta \cos H$
where $\sin\delta \approx \sin\varepsilon \sin\lambda + \sin i \sin u$
R_Z and R_S are the polar and equatorial components of the station vectors (Fig. 6), and H is the local hour angle of the reflector. The declination δ depends on the obliquity (ε), lunar longitude measured from the equinox (λ), lunar orbit inclination i, and

angle between Moon and its node on the ecliptic (u). Consequently, sensitivity to these quantities comes from the projection of the station vector along the Earth-Moon direction.

19. K. Nordtvedt, *Phys. Rev.* **170**, 1186 (1968).

20. C. M. Will, *Theory and Experiment in Gravitational Physics*, Cambridge Univ. Press (1981).

21. See for example, C. Brans and R. H. Dicke, *Phys. Rev.*, **124**, 925 (1961).

22. I. I. Shapiro, C. C. Counselman, III, and R. W. King, *Phys. Rev. Let.* **36**, 555 (1976); J. G. Williams, R. H. Dicke, P. L. Bender, *et al.*, *Phys. Rev. Let.* **36**, 551 (1976).

23. U_G is the gravitational self-energy of the body, $U_G = -\frac{G}{2}\int\frac{\rho(x)\rho(x')dVdV'}{|x-x'|}$, where $\rho(x)$ is the density, **x** is the position vector and V indicates volume.

24. K. Nordtvedt, *Phys. Rev. D.* **37**, 1070 (1988).

25. To achieve what are usually called realistic errors, solutions involving a number of different subsets of the data and of the parameters have been carried out to investigate the stability of the results. In addition, a hypothetical 1 cm cos D systematic range error has been included.

26. J. O. Dickey, X X Newhall, and J. G. Williams, *Adv. Space Res. 9* **No. 9**, 75 (1989).

27. I. I. Shapiro, in *General Reltivity and Gravitation*, 1989, N. Ashby, D. F. Bartlett, and W. Wyss, Eds., Cambridge Univ. Press (1990).

28. R. D. Reasenberg *et al.*, *ApJ. Lett.* **234**, L219 (1979).

29. B. Bertotti, I. Ciufolini and P. L. Bender, *Phys. Rev. Let.* **58**, 1062 (1987).

30. I. I. Shapiro, R. D. Reasenberg, J. F. Chandler, and R. W. Babcock, *Phys. Rev. Lett.* **61**, 2643 (1988).

31. The lunar J_2 uncertainty dominates, contributing 0.7% to the error.

32. D. La and P. J. Steinhardt, *Phys. Rev. Lett.* **62**, 376 (1989).

33. J. F. Chandler, R. D. Reasenberg, and I. I. Shapiro, *Bull. Amer. Astron. Soc., 25,* p. 1233 (1993).

34. R. W. Hellings *et al.*, *Phys. Rev. Lett.* **51**, 1609 (1983).

35. T. Damour, G. W. Gibbons, and J. H. Taylor, Phys. Rev. Lett. 61, 1151 (1988); J. H. Taylor and J. M. Weisberg, *Astrophys. J.* **345**, 434 (1989).

36. R. Hide and J. O. Dickey, *Science* **253**, 629, and references therein (1991).

37. M. Feissel and D. C. Gambis, *r. hebd. Seanc. Acad. Sci., Paris* **B291**, 271 (1980); R. B. Langley, R. King, I. I. Shapiro, R. D. Rosen, D. A. Salstein, *Nature* **294**, 730 (1981).

38. J. D. Anderson and R. D. Rosen, *J. Atmos. Sci.* **40**, 1584 (1983); R. A. Madden, *J. Geophys. Res.*, **93**, 5333 (1988); R. A. Madden, *J. Geophys. Res.* **92**, 8391 (1987); J. O. Dickey, M. Ghil, S. L. Marcus, *J. Geophys. Res.* **96**, 22,643 (1991); M. Ghil and K. Mo, *J. Atmos. Sci.* **48**, 752 (1991).

39. C. F. Yoder, J. G. Williams, M. E. Parke, *J. Geophys. Res.* **86**, 881 (1981).

40. A. J. Ferrari W. S. Sinclair, W. L. Sjogren, J. G. Williams, *J. Geophys. Res.* **85**, 3939 (1980).

41. J. C. Ries, R. J. Eanes, C. K. Shum, M. M. Watkins, *Geophys. Res. Lett.* **19**, 529 (1992).

42. K. Lambeck, The Slow Deformation of the Earth, *Geophysical Geodesy*, Clarendon Press, Oxford, (1988).

43. J. G. Williams, W. S. Sinclair, and C. F. Yoder, *Geophys. Res. Let.*, **5**, 943-946 (1978).

44. J. G. Williams, X X Newhall, J. O. Dickey, *EOS Trans., AGU,* **73** (43), 126 (1992).

45. J. G. Marsh *et al., J. Geophys. Res.* **95**, 22,043 (1990); M. K. Cheng, R. J. Eanes, and B. D. Tapley, *Geophys. J. Int.*, **108**, p. 401 (1992).

46. C. F. Yoder, *Phil. Trans. R. Soc. London A303* 327 (1981).

47. C. F. Yoder, in *Natural and Artificial Satellites* (eds. P. E. Nacozy and S. Ferraz-Mello), Univ. of Texas Press, 211-221 (1979).

48. J. G. Williams, X X Newhall, J. O. Dickey, *Astron. Astrophys.* **241**, L9-L12 (1991).

49. T. A. Herring, C. R. Gwinn, I. I. Shapiro, *J. Geophys. Res.* **91**, 4745 (1986); W. E. Himwich and E. J. Harder, in *The Earth's Rotation and Reference Frames for Geodesy and Geodynamics*, A. K. Babcock and G. A. Wilkins, Eds. (Kluwer,

Dordrecht, 1988), pp. 301-307; S. Y. Zhu, E. Groten, C. Reigber, *Astron. J.* **99**, 1024 (1990); J. A. Steppe, S. O. Oliveau, O. J. Sovers, in *IERS Technical Report No. 5*, M. Feissel, Ed. (Observatoire de Paris, Paris, 1990), pp. 13-24; T. A. Herring, B. A. Buffet, P. M. Mathews, I. I. Shapiro, *J. Geophys. Res.* **96**, 8259 (1991).

50. C. R. Gwinn, T. A. Herring, I. I. Shapiro, *J. Geophys. Res.* **91**, 4745 (1986).

51. J. Hinderer, D. Jault, H. Legros, J-L Le Mouël, *Phys. Earth Planet. Interiors* **59**, 329 (1990).

52. P. Charlot, O. J. Sovers, J. G. Williams, X X Newhall, *Proceedings of the 127th Colloquium of the International Astronomical Union, Reference Systems,* 228 (U. S. Naval Observatory, Washington, C. A. Smith, and G. H. Kaplan, 1991).

53. J. G. Williams, X X Newhall, J. O. Dickey, *Lunar Gravitational Harmonics and Reflector Coordinates, Proc. Intern. Symp.: Figure and Dynamics of the Earth, Moon and Planets, special issue of the Monograph Series of the Research Institute of Geodesy, Topography and Cartography*, P. Holota, Ed., pp. 643-648 (1987); R. W. King, C. C. Counselmann III, I. I. Shapiro, *J. Geophys. Res.*, **81**, 6251 (1976); M. E. Davies, T. R. Colvin, D. L. Meyer, *J. Geophys. Res.*, **93**, 14177 (1987).

54. A. S. Konopliv, W. L. Sjogren, R. N. Wimberly, R. A. Cook, and A. Vijayaraghavan, AAS 93-622 at AAS/AIAA Astrodynamics Specialist Conference (1993).

55. W. J. Eckert, *Astron. J.*, **70**, 787-792 (1965); N. Borderies and C. F. Yoder, *Astron. and Astrophys.*, **233**, 1, 235-251 (1990). Nodal contribution = $-3/2n\ (R/a)^2 \sin(I+\varepsilon)/\sin I\ (J_2 + 2C_{22}) = -0.17$ arcseconds/year, where n is the mean motion, R/a the ratio of lunar radius to semimajor axis, ε the obliquity, and I the orbital inclination.

56. C. T. Russell, P. J. Coleman, Jr., B. E. Goldstein, *Proc. Lunar Planet. Sci.* **128**, 831 (1981).

57. M. J. Wiskerchen and C. P. Sonnett, *Proc. Lunar Sci. Conf.*, 515-535 (1977).

58. Y. Nakamura, *J. Geophys. Res.* **88**, 677-686 (1983).

59. D. H. Eckhardt, *Moon and the Planets* **25**, 3-49 (1981).

60. $x = \frac{(a-c)}{a}\left(\frac{18.6\ yr}{27.3d}\right) = \frac{e_c}{0.0040}$

61. N. R. Goins, N. M. Toksoz and A. M. Dainty, *Proc. Lunar Planet Sci.*, 2424 (1979); and N. R. Goins, A. M. Dainty, and M. N. Toksöz, *J. Geophys. Res.* **86**, 5061-5074 (1981).

62. $\Delta k = k_2(400\ km) - k_2(300\ km) \simeq 0.001$.

63. The core frictional parameter y is related to the friction coupling parameter K by

$$y = K\left(\frac{18.6yr}{27.3d}\right) = \frac{K}{0.0040},$$

where the frictional torque is $KI_c\,\omega(\omega-\omega_c)$ and ω and ω_c are the angular velocity vectors of mantle and core, respectively. For turbulent skin friction, $K = (45\pi/32)\kappa \sin\Delta\varepsilon$. Here, $\Delta\varepsilon$ is the differential obliquity of core and mantle spin vectors and is approximately equal to mantle obliquity (1.52°) for weak frictional and Pioncaré pressure coupling. In turn, the local skin friction parameter κ can be derived using simple flat plate theory and is of order 0.001 to within a factor of 2. A 350km core radius (with core density = 7g/cc) corresponds to $\kappa = 0.0016$.

64. The contribution of solid friction in the Moon to the secular dn/dt is

$$\frac{dn}{dt} \approx \frac{9}{2}\frac{k_2}{Q}\frac{M_{EARTH}}{M}\left(\frac{R}{a}\right)^5 n^2(7e^2 + \sin^2(I+\varepsilon)) = 0.4\text{arcsec/century}^2$$

where e is the orbital eccentricity.

65. O. Calame, *Scientific Applications of Lunar Laser Ranging*, J. D. Mulholland, Ed. (Reidel, Dordrecht, 1977), pp. 53-63; R. J. Cappallo, R. W. King, C. C. Counselman, III, I. I. Shapiro, *Celestial Mechanics,* **26**, 145 (1982); and J. G. Williams, X X Newhall, J. O. Dickey, *EOS, Trans. Amer. Geophys. Union* **72**, 17, 179 (1991); D. H. Eckhardt, *Cel. Mech. and Dyn. Astron.*, **57**, 307-324 (1993).

66. S. J. Peale, *J. Geophys. Res.* **81**, 1813 (1976).

67. P. L. Bender, in *Refraction of Transatmospheric Signals in Geodesy* (eds. J. C. De Munck, and T. A. Th. Spoelstra), Netherlands Geodetic Commission No. 36, 117-125 (1992); T. A. Herring, ibid, 157-164 (1992). The total atmospheric correction uncertainty given by Bender in Case II of Table 1 is 2 mm at 45° elevation, with one of the two largest contributions being from uncertainties in horizontal gradients. The horizontal gradient effect assumed for Case II is just equal to the total tropospheric horizontal gradient effect for radio waves found by Herring from extensive VLBI measurements. The horizontal gradient contribution should be smaller for laser propagation than for radio waves.

68. Bender, P. L. *et al.*, *Astrophysics from the Moon, AIP Conference Proceedings 207*, eds.: M. J. Mumma, H. J. Smith, and G. H. Linebaugh, American Institute of Physics, New York, 647-653, (1990).

We wish to acknowledge and thank E. C. Silverberg for his pioneering efforts at McDonald Observatory in the early years of the LLR experiment. Major contributions were made by C. O. Alley, D. G. Currie, and J. D. Mulholland. The success of the early program would not have been possible without the strong support of the late Harlan J. Smith. We also acknowledge the staffs at CERGA, Haleakala, and McDonald Observatory. Normal points were constructed from individual photon returns by R. Ricklefs, P. Shelus, A. Whipple, and J. G. Ries at the University of Texas at Austin for the MLRS and for earlier Haleakala data. D. O'Gara produced later Haleakala normal points. C. Veillet provided normal points for the CERGA data. The work of three of the authors (J. O. Dickey, X X Newhall and J. G. Williams) presents the results of one phase of research carried out at the Jet Propulsion Laboratory, California Institute of Technology, under contract with the National Aeronautics and Space Administration. The University of Texas authors (R. L. Ricklefs, J. G. Ries, P. J. Shelus, A. L. Whipple, and J. R. Wiant) acknowledge support from the National Aeronautics and Space Administration and the U. S. Naval Observatory.

Table 1. Distribution of LLR Data

Observatories	Apollo 11	Apollo 14	Apollo 15	Lunakhod 2	Total Number of Normal Points
McDonald Observatory 2.7m (Texas)	468	495	2356	132	3451
McDonald Laser Ranging System (MLRS)	24	36	607	5	672
Halaekala (Maui, HI)	20	23	633	18	694
CERGA (Grasse, France)	324	339	2699	197	3559

Table 2. Solution Parameters

Calibration
- Bias in each station
- Bias in individual spans of data

Earth
- Station coordinates
- Monthly and fortnightly tidal terms in Universal Time (UT1)*
- Rate correction in UT1 and polar motion
- Precession and obliquity rate
- Nutation terms at 18.6 yr, 1 yr*, 1/2 yr*, 1/2 month*, and free core nutation*

Orbit
- Lunar orbit
- Solar orbit
- GM Earth + Moon
- Tidal acceleration
- Geodetic precession
- Nordtvedt coefficient

Moon
- Reflector coordinates—4 sites
- Six libration initial conditions
- Second degree moment difference—β, γ
- J_2 and Third degree harmonics
- Lunar rotational dissipation
- Lunar Love number
- Experimental libration terms*

Earth Rotation Parameter solved for stochastically:
- Universal Time
- Variation of Latitude/Polar Motion

*Terms that are not normally included in a standard solution.

Table 3. Determination of Gravitation Physics and Relativity Parameters

Nordtvedt Effect
$\eta = -0.0006 \pm 0.0014$
$C_0\eta = -0.5 \pm 1.3$ cm

Parametrized Post Newtonian (PPN) Parameter
$\beta = 0.9999 \pm 0.0006$

Deviation from the Expected Geodetic Precession
$-0.3 \pm 0.9\%$

Table 4. Determination of Geophysical Parameters

GM_{EARTH}	$398{,}600.442 \pm 0.004$ km^3/sec^2
Luni-Solar Precession constant	50.3845 ± 0.0004 arcsec/year
18.6 yr nutation corrections (units: milliarcseconds)	
In-phase terms	
$\Delta\varepsilon$	2.8 ± 1.1
$\sin\varepsilon\,\Delta\varepsilon$	-2.9 ± 1.4
Out-of-phase terms:	
$\Delta\varepsilon$	0.6 ± 1.3
$\sin\varepsilon\,\Delta\varepsilon$	0.5 ± 1.0
$\dot{n}$ secular acceleration of the Moon	
Total	-25.88 ± 0.5 arcsec/cy^2
Diurnal term	-4.04 ± 0.4 arcsec/cy^2
Semi-diurnal term	-22.24 ± 0.6 arcsec/cy^2
Lunar contribution	$+0.40$ arcsec/cy^2
Increase Semi-major axis rate	3.82 ± 0.07 cm/year

Figure Captions

1. Photograph of a retroreflector array of Apollo 14 on the lunar surface.

2. Geographical distribution of the retroreflector arrays on the lunar surface, A-11, A-14 and A-15 denote the Apollo 11, 14 and 15 site, respectively; whereas L-1 and L-2 are the Lunakhod 1 and 2 locations (no returns are available from Lunakhod 1).

3 Histogram of the weighted root-mean square (rms) residual as a function of time.

4. The McDonald Laser Ranging System atop Mt. Fowlkes.

5. Histogram of LLR normal points as a function of year. The years 1982 and 1983 marked the transition from the McDonald 2.7m telescope observing program to the McDonald Laser Ranging System.

6. The geometry of the Earth-Moon System.

7. Lunar orbit about the Earth as affected by the Nordtvedt term. A violation of the Equivalence Principle would cause the orbit of the Moon about the Earth-Moon center of mass to be polarized in the direction of the Sun, with the maximum size of ~ 9 m.

8. Constraint on core radius from moment of inertia and lower mantle density contrast.

9. Love number k_2 as a function of Apollo derived S-wave velocity profiles of Goins *et al.* (61) and Nakamura (58); comparison of LLR-determined value of k_2 is made with that derived from variable V_s below 1000 km depths and core radius of 300 and 400 km. Note that LLR value is independent of V_s.

10. Orientation of the Moon relative to the Cassini state.

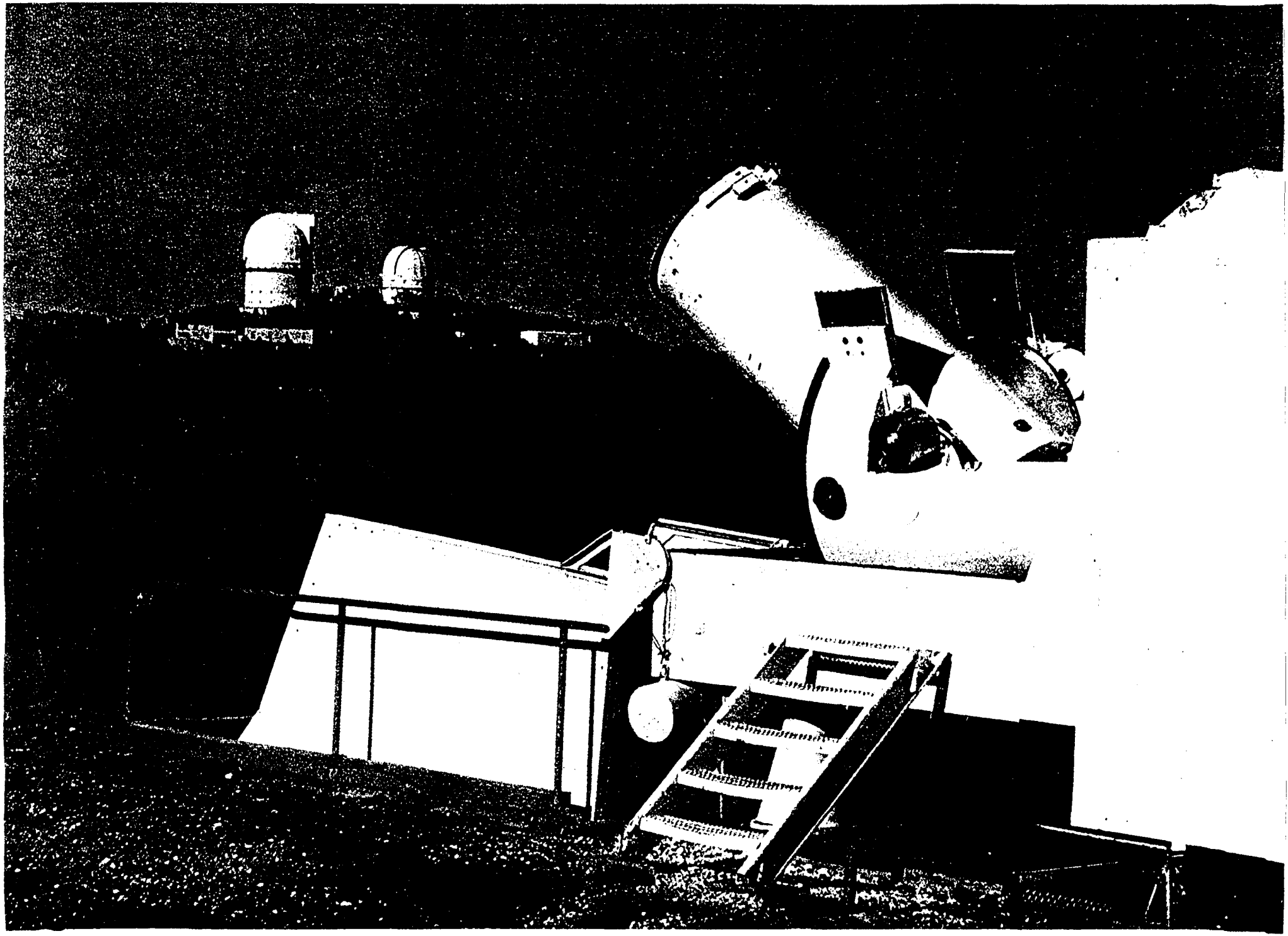

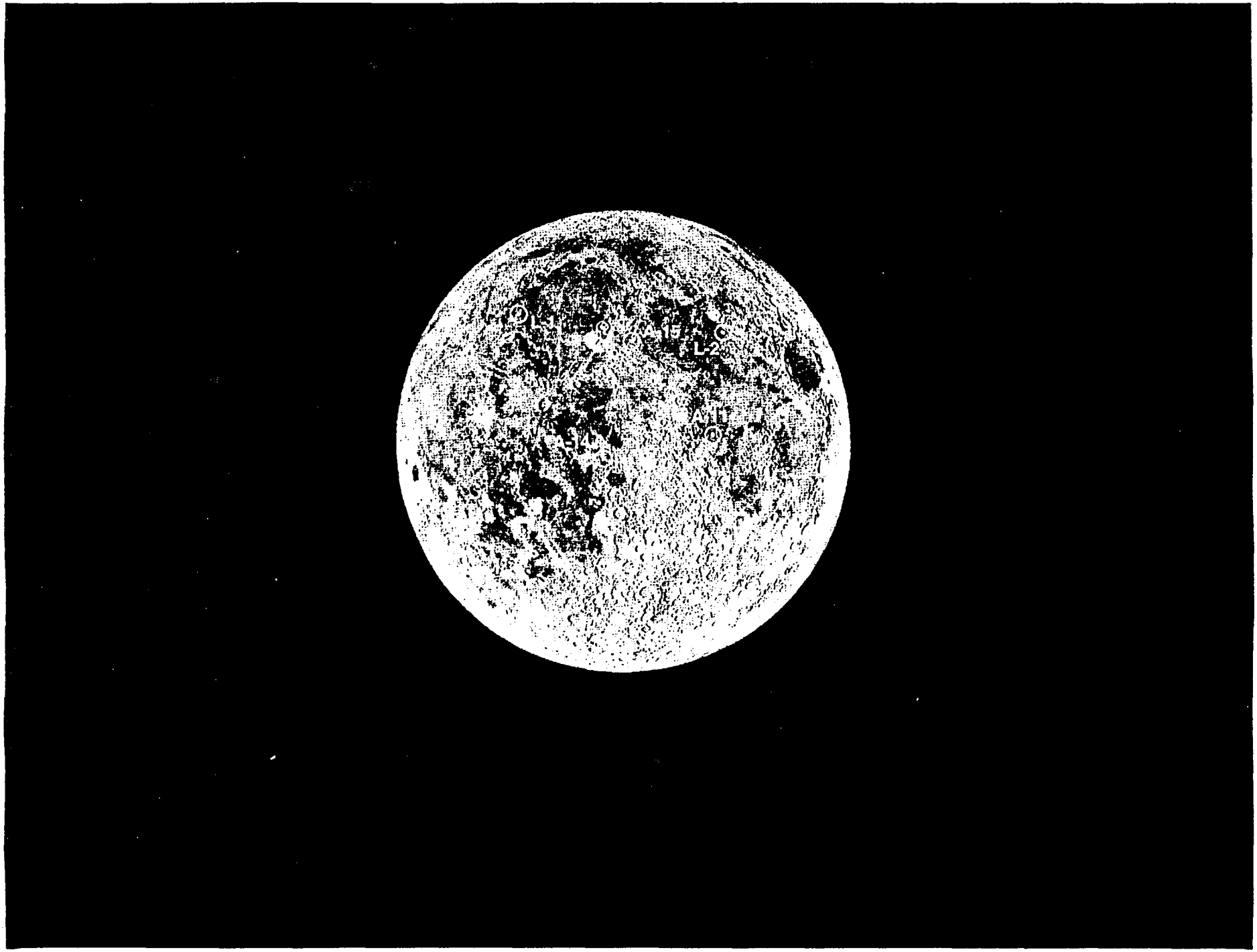
L2

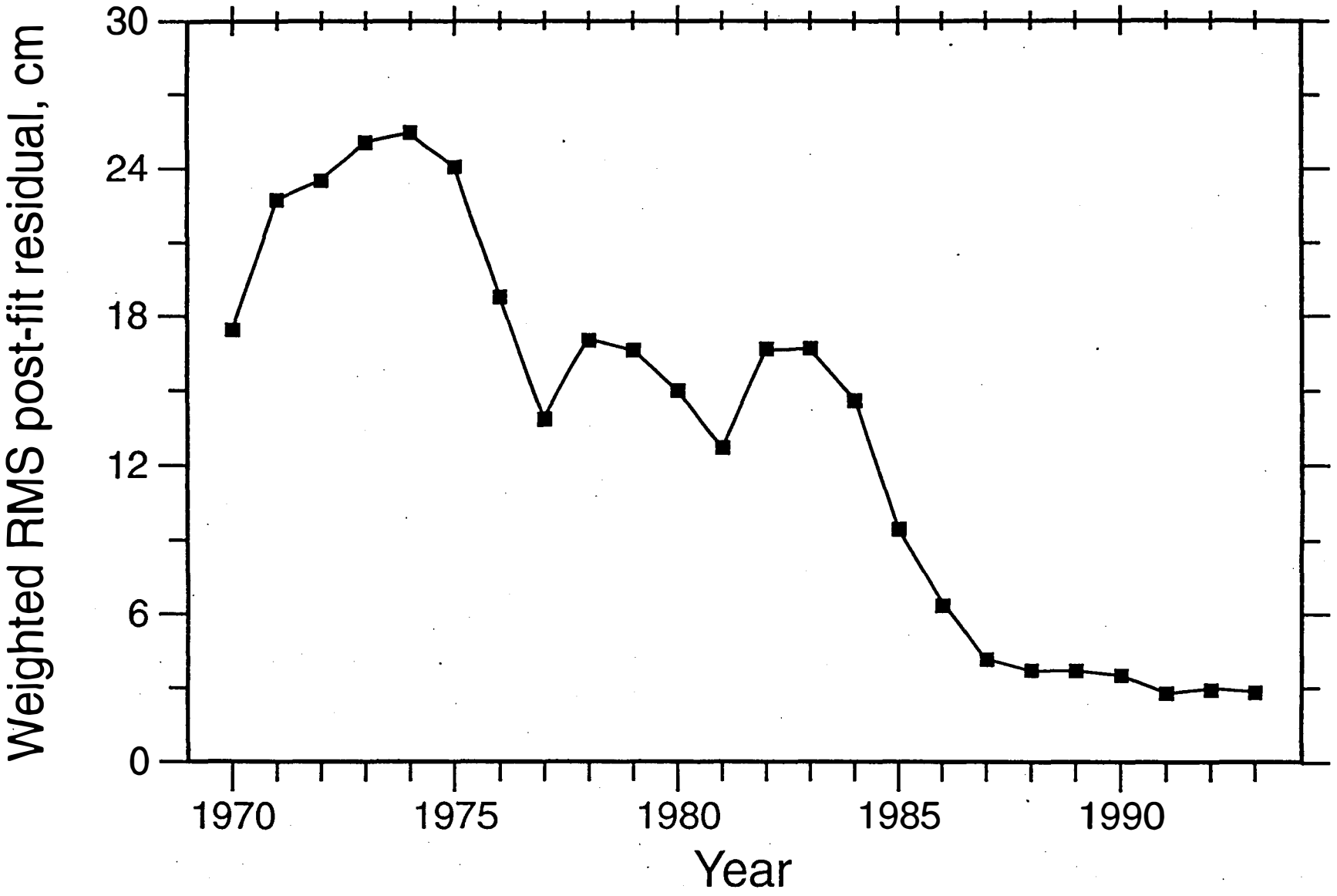
Weighted RMS post-fit residual, cm
30
24
18
12
6
0
1970
1975
1980
1985
1990
Year

Fig 3

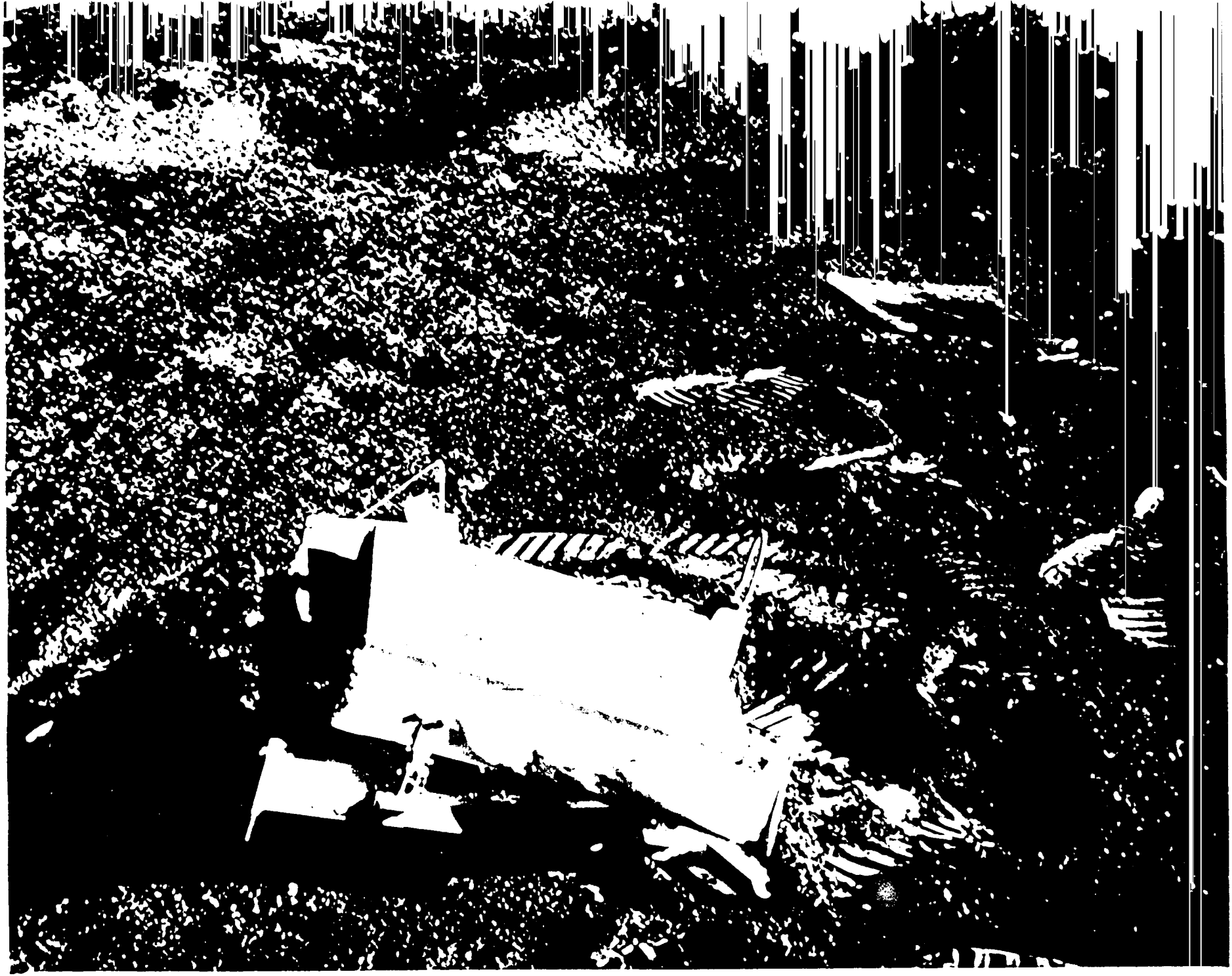

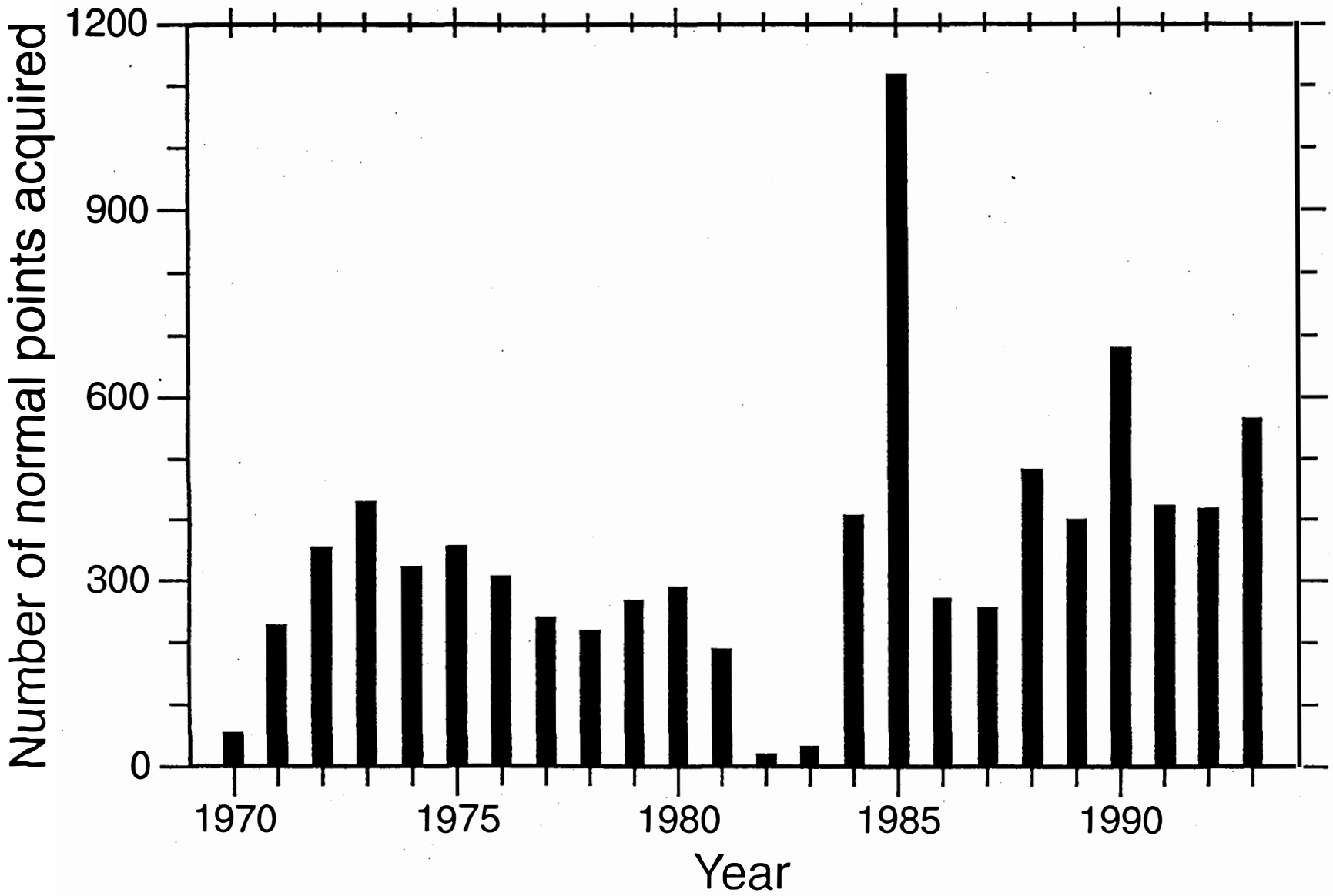
Number of normal points acquired
1200
900
600
300
0
1970
1975
1980
1985
1990
Year

Fig 5

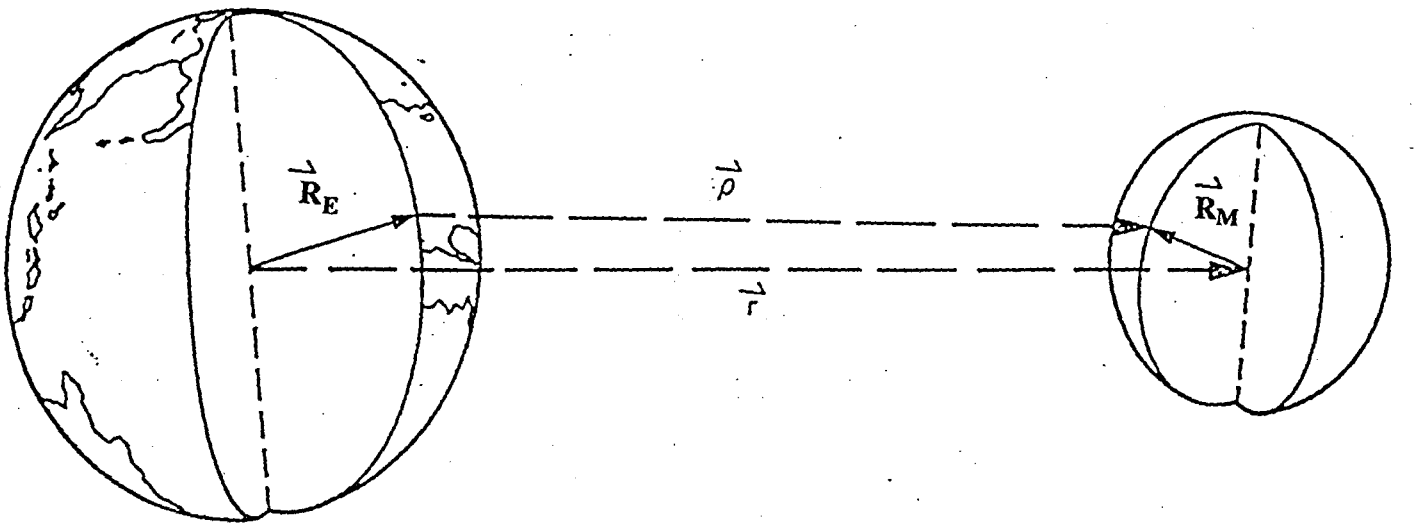

Fig. 6

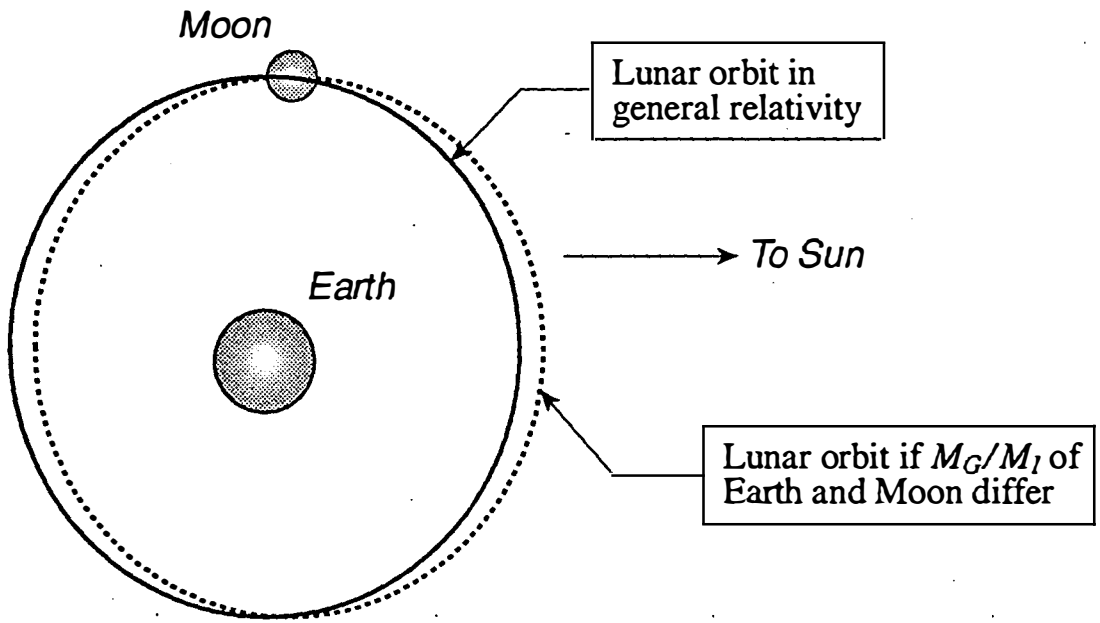
Moon
Lunar orbit in general relativity
To Sun
Earth
Lunar orbit if M_G/M_I of Earth and Moon differ

Fig 7

Lunar Density Profile

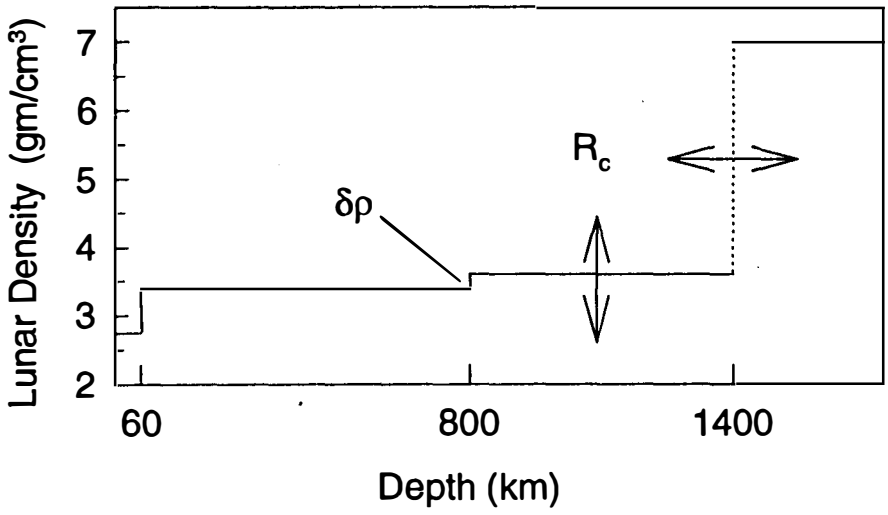

Core Radius versus lower mantle density contrast

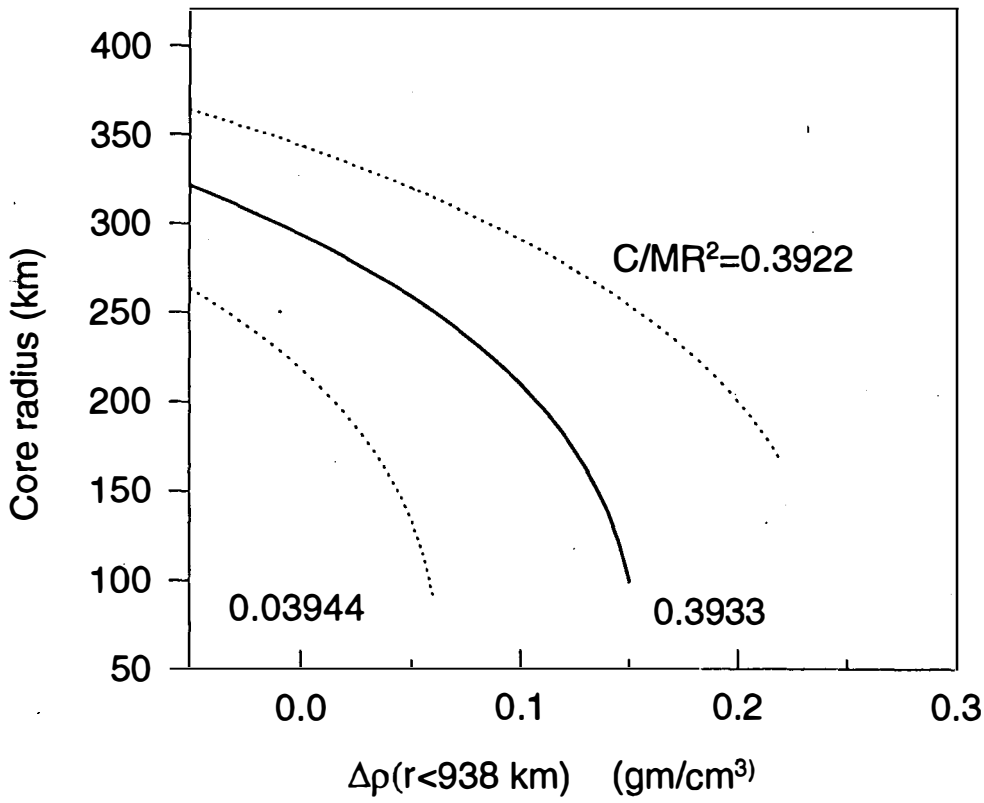

Fig 8

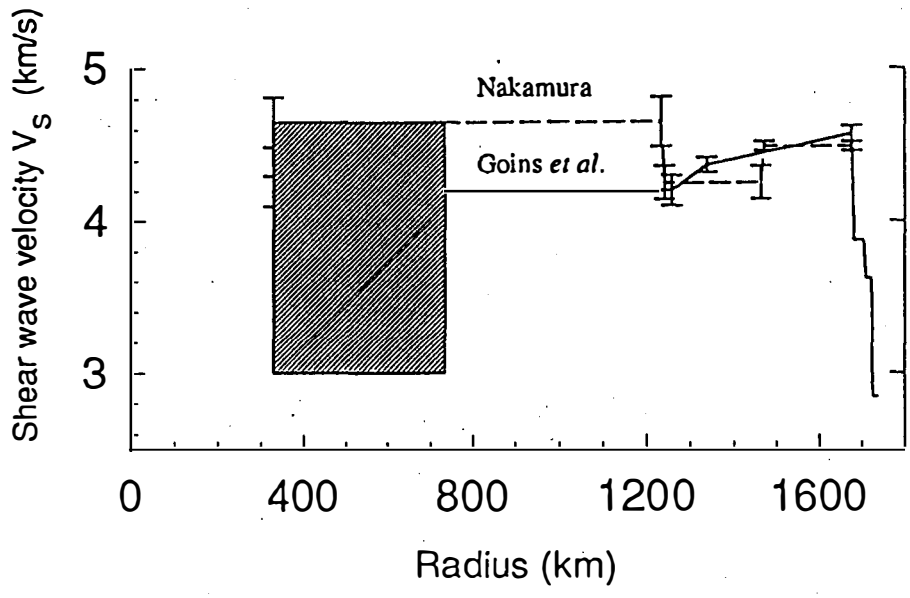
Shear wave velocity V_S (km/s)
5
4
3
Nakamura
Goins *et al.*
0
400
800
1200
1600
Radius (km)

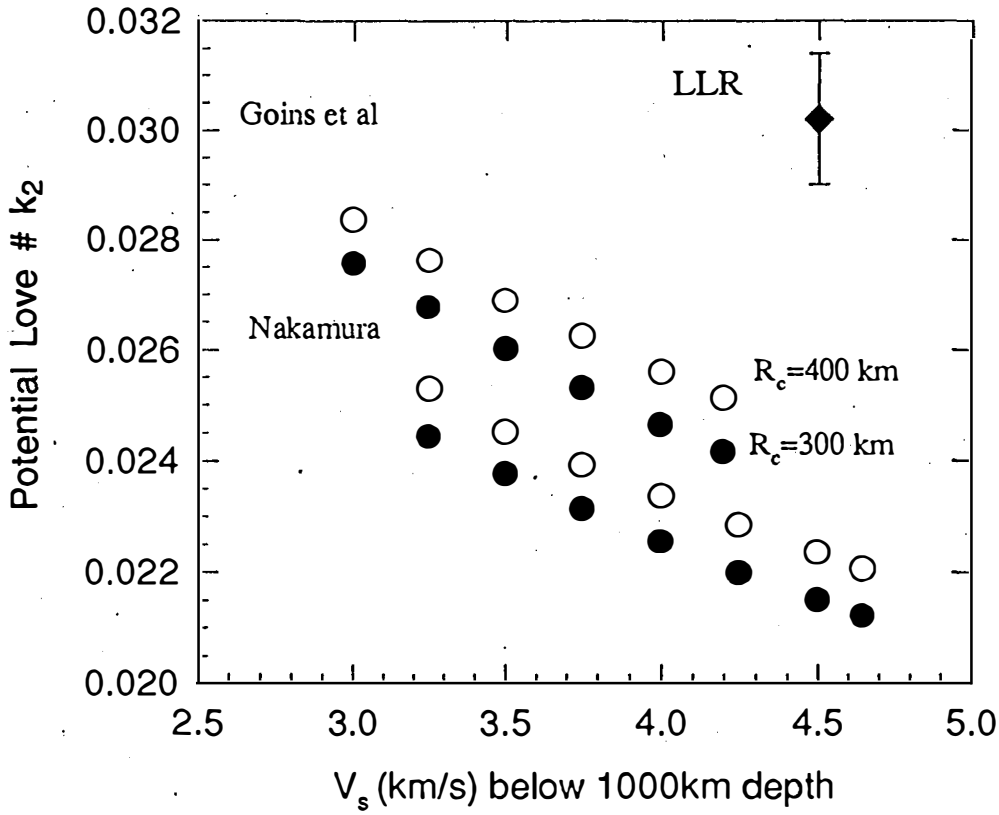
Potential Love # k_2
0.032
0.030
0.028
0.026
0.024
0.022
0.020
Goins et al
LLR
Nakamura
R_c=400 km
R_c=300 km
2.5
3.0
3.5
4.0
4.5
5.0
V_s (km/s) below 1000km depth

Fig 9

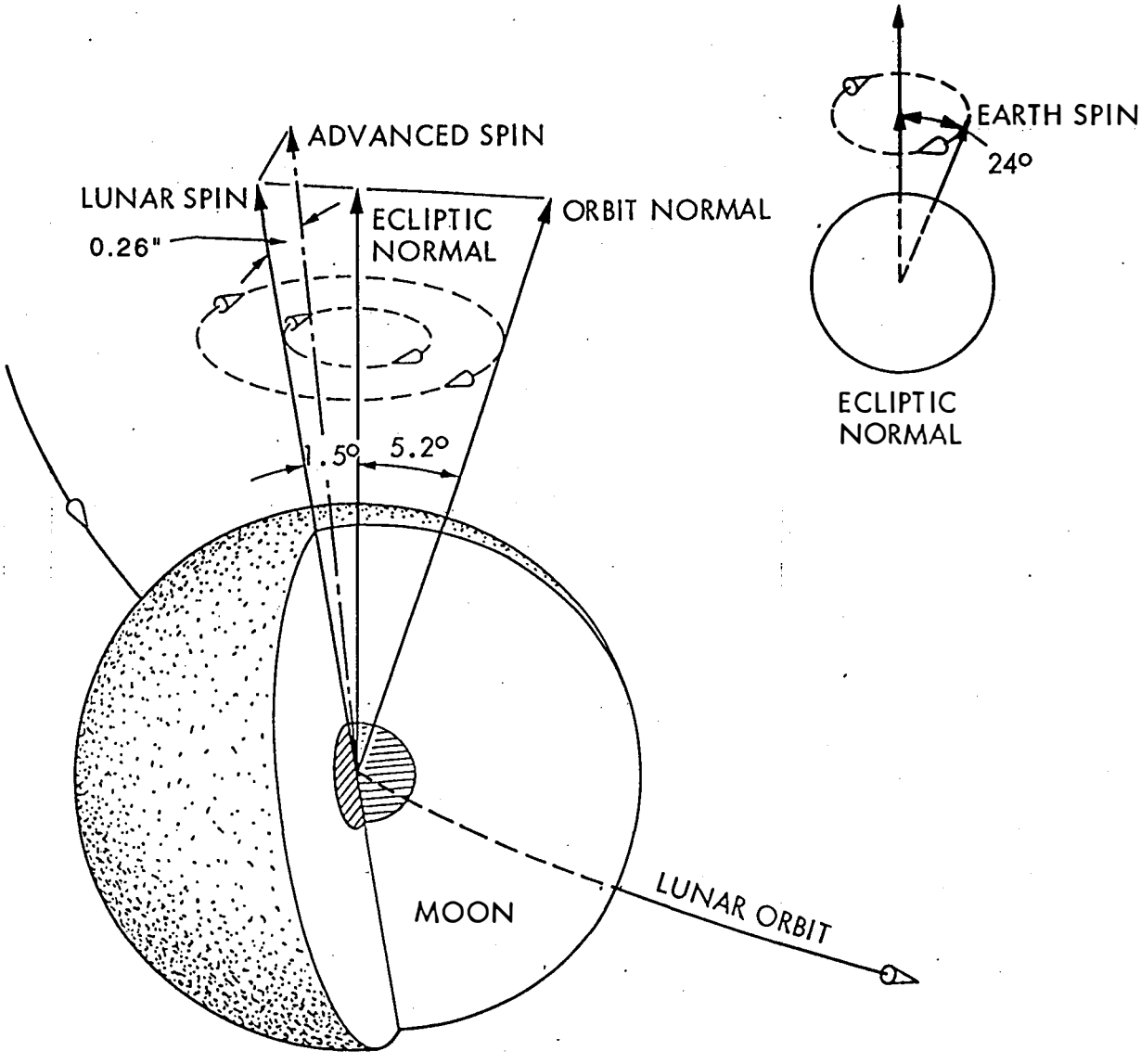
ADVANCED SPIN
LUNAR SPIN
0.26"
ECLIPTIC
NORMAL
ORBIT NORMAL
1.5°
5.2°
MOON
LUNAR ORBIT
EARTH SPIN
24°
ECLIPTIC
NORMAL

Fig 10